Thermal-Blooming Laboratory Experiments

Bernadette Johnson

We conducted a multiphase series of laboratory experiments to explore the adaptive optics compensation of a laser beam distorted by strong thermal blooming. Our experimental approach was to create on a small, low-power beam the same phase distortion that would be experienced by a large, high-power beam propagating through the atmosphere and to apply phase compensation via deformable mirrors. We performed the investigations to lay the foundation for future ground-based laser experiments and their corresponding atmospheric-propagation computer models.

The experiments had three primary objectives: to provide a controllable, repeatable means of obtaining data for the verification and benchmarking of computer codes, to investigate the different phase-compensation instability (PCI) mechanisms that were predicted by theory and computer code, and to gain information relevant to the design of adaptive optics systems for ground-based laser propagation. The experiments were successful in realizing all three objectives: we observed the first experimental evidence of PCI and achieved excellent agreement between experimental results and computer-code predictions. In addition, the work provided valuable insight to the role of adaptive optics hardware in influencing high-energy beam propagation and to the importance of incorporating realistic hardware models into propagation codes.

One of the goals of the Strategic Defense Initiative Organization (SDIO), formed in the mid-1980s, was to establish the feasibility of using ground-based lasers to intercept ballistic missiles. For ground-based lasers to be useful in this type of mission, it was necessary to show that atmospheric compensation could be performed for a very-high-energy laser beam propagating from the ground to an orbiting relay mirror.

At the time that this SDIO research was initiated, Lincoln Laboratory was completing the Atmospheric-Compensation Experiments (ACE), described by Darryl P. Greenwood et al. [1] and Daniel V. Murphy [2] in this issue, and was actively planning for the Short-Wavelength Adaptive Techniques (SWAT) experiments, described by Ronald A. Humphreys et al. [3] and Byron G. Zollars [4] in this issue. Although these experiments demonstrated ground-to-space compensation, they addressed only compensation for turbulence because they used only low-power beams. For high-energy beams it is also necessary to compensate for thermal blooming—spreading of the beam that results from energy deposited in the atmosphere by the laser beam itself.

From our early work in the 1970s on the thermal-blooming compensation of focused laser beams [5–7], we knew that adaptive optics could not always provide a perfect correction for thermal blooming. Although correction of beams propagated from the ground to space is actually easier than correction of beams focused in the atmosphere, the fundamental nonlinearity of the thermal-blooming effect can lead

to instabilities [8–10] that limit the correction, particularly at the extraordinarily high energies required for ballistic-missile defense. In fact, some researchers suggested that thermal blooming could not be corrected in the high-energy SDIO scenario, thus making ground-based lasers unsuitable for such an application.

To investigate the correctability of thermal blooming for the SDIO scenario, Lincoln Laboratory conducted a three-part program that involved

1. theoretical analyses and the development of a time-dependent propagation computer code called MOLLY [11],
2. laboratory experiments scaled to real atmospheric scenarios, and
3. a horizontal-path field experiment [12].

The scaled laboratory experiments are the subject of this article.

We conducted the laboratory experiments in two phases. In Phase I, which used a 69-channel adaptive optics system, we obtained the first experimental evidence of thermal-blooming phase-compensation instability (PCI) by seeding the instability with an initial intensity perturbation [13]. In Phase II, which used a 241-channel adaptive optics system, we observed the first experimental evidence of the spontaneous growth of thermal-blooming PCI [14].

Although we did observe the predicted PCI phenomenon, we discovered that the instability was actually difficult to excite; careful adjustment of laboratory conditions was required. Our results showed that adaptive optics can provide a good, stable correction for thermal blooming under most conditions. We compared our laboratory results to the predictions of the MOLLY propagation code, and by benchmarking the code in this way we were able to corroborate its predictions that thermal blooming can be successfully corrected for a ground-to-space path of a laser beam at full ballistic-missile-defense power levels.

Motivation

Theoretical work in the phase compensation of thermal blooming predicted limits to high-energy beam propagation based on the degrading effects of various instabilities. These instabilities included PCI, which is caused by feedback of the adaptive optics system, and turbulence/thermal-blooming interaction (TTBI), in which small-scale blooming of turbulent scintillations leads to a scattering loss of energy from the beam.

Figure 1 explains the mechanism of PCI. The figure schematically shows the intensity distribution within a laser beam as it propagates from the ground to the top of the atmosphere at three successive times in the process of an adaptive optics phase correction. (For an introduction to adaptive optics concepts, see the article by Greenwood [1] in this issue.) The high-energy laser beam is assumed to have regions of local intensity maxima, or "hot spots," which are represented by the darker zones in Figure 1. (Hot spots can arise, for example, from turbulence-induced scintillations or from an inherent structure in the beam as it emerges from the laser.)

When a laser beam propagates through the atmosphere, the atmosphere absorbs some of the energy and becomes warmer where the beam is most intense. As a result, just milliseconds after the beam is turned on, the air becomes less dense in these regions, thus causing local changes in the refractivity of the atmosphere. When light from a beacon in space passes down through the region where the high-energy laser beam is present, the beacon wavefront, which is initially flat, develops wiggles that match the refractivity pattern produced in the atmosphere by the laser-induced heating (Figure 1[a]).

A wavefront sensor measures the structure of the beacon phase, and when the adaptive-optics-system loops are closed, the conjugate of this phase structure is placed on the outgoing laser beam by the deformable mirror. (We have assumed that the deformable mirror was initially flat.) It turns out, however, that the mirror will actually focus energy into regions that were already the warmest, thereby heating them even more (Figure 1[b]). As a result, the refractivity pattern in the atmosphere becomes even more concentrated. The beacon radiation brings this information to the wavefront sensor, the compensation system again tries to correct for the phase error, which is now larger than the initial error, and the deformable mir-

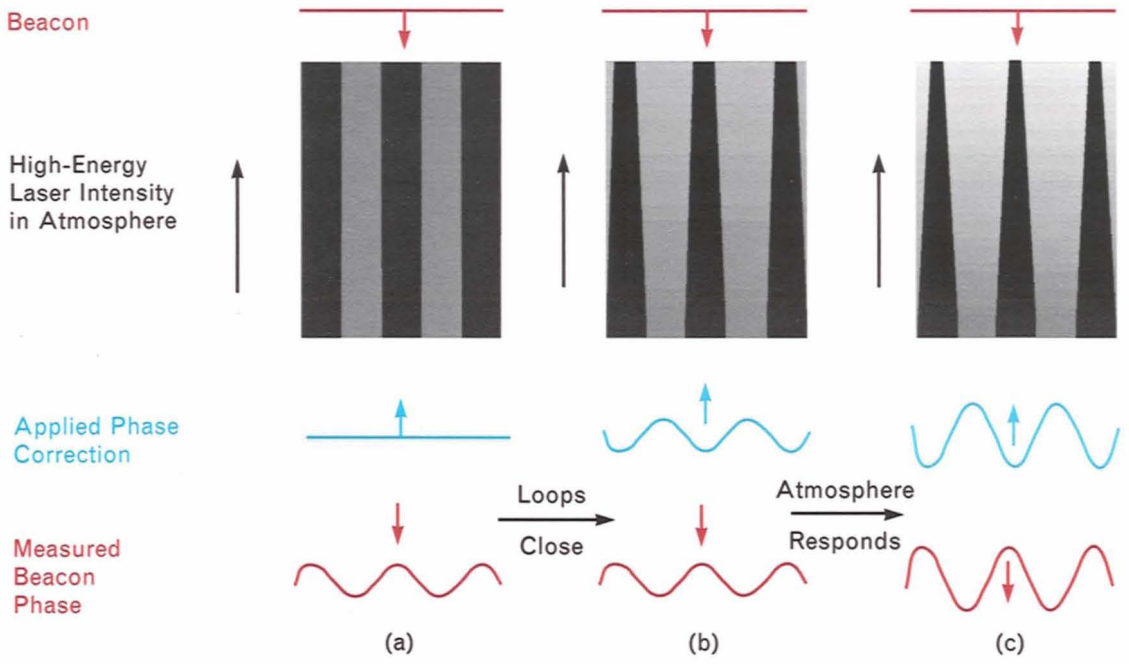

FIGURE 1. Phase-compensation instability (PCI) mechanism: (a) When light from a beacon in space passes down through a region where a high-energy laser beam is present, the beacon wavefront develops wiggles that match the refractivity pattern produced in the atmosphere by the laser-induced heating. (b) A deformable mirror in the system places the conjugate of this phase structure on the outgoing laser beam. As it turns out, the mirror will then focus energy into regions that were already the warmest, thereby heating them even more. (c) Thus the refractivity pattern in the atmosphere becomes even more concentrated, the compensation system again tries to correct for this phase error, which is larger than the initial error, and the deformable mirror causes the local structure in the laser beam to focus energy even more strongly into the warmest regions. (Note: Local intensity maxima, or "hot spots," are represented by darker zones.)

ror causes the local structure in the laser beam to focus even more strongly (Figure 1[c]).

Clearly this situation is unstable—the intensity in these regions, as well as the phase corrections, will continue to grow until they are limited by the hardware or by some other saturation mechanism. In this discussion, we have ignored the effects of wind (natural and slew-induced) as well as any temporal changes in the atmosphere and any finite time delays of the adaptive optics system. These factors all play a role in determining how the interaction between the adaptive optics correction and the atmosphere will evolve.

TTBI is a specific case of a more general open-loop phenomenon that has also been referred to as stimulated thermal Rayleigh scattering (STRS) [15]. TTBI occurs when the spatial scales of phase aberrations associated with irradiance hot spots are too small for the adaptive optics system to compensate; i.e., the spatial scales are smaller than the correction system's spatial Nyquist frequency, which is equal to two actuator spacings. In TTBI, the hot spots can cause local atmospheric heating that scatters energy out of the beam. If the atmosphere is thick enough and the hot spots small enough, the hot spots can grow and their growth will eventually saturate by diffusion, thermal blooming (spreading) of the whole beam, or wind clearing.

The growth rates for both PCI and TTBI increase with increasing thermal-blooming distortion and decreasing hot-spot size [9, 10]. Time-dependent propagation codes developed both within and outside Lincoln Laboratory have predicted rapid degradation in beam quality as a function of laser energy, due largely to the effect of PCI and TTBI. Although we have also

investigated TTBI in the laboratory, we will deal only with PCI in this article.

In their early stages of development, time-dependent codes were viewed with skepticism for several reasons. First, and perhaps most importantly, no experimental verification of theoretical or code predictions existed. Second, although some emphasis was placed on incorporating realistic atmospheric models into the codes, little attention was paid initially to modeling the adaptive optics hardware or to understanding the role of the hardware in estimating system performance. Consequently, we designed a two-phase set of laboratory thermal-blooming experiments to address these concerns. The objectives of these experiments were threefold:

1. to provide a controllable, repeatable source of data to verify and benchmark code predictions,
2. to observe, understand, and characterize the different instability mechanisms that were predicted by theory and code, and
3. to gain information relevant to the design of the adaptive optics systems for ground-based laser propagation.

While the laboratory experiments were under way, the time-dependent code was upgraded to include specific features of the experimental hardware. In this way, experimental conditions were used as code inputs and results of the two could be easily compared. This parallel effort, which was unique among research groups involved in laser propagation through the atmosphere, yielded interesting results that will be discussed in subsequent sections.

Experimental Approach

The experiments proceeded in two phases: the first phase used the 69-channel adaptive optics system that had been developed for the ACE program (see the article by Greenwood [1] in this issue) and the second used a new 241-channel system that was constructed specifically for these experiments. Both phases of experimentation used two deformable mirrors, mainly to increase the total amount of phase distortion that could be compensated, but also to explore alternate compensation schemes, such as a woofer-tweeter approach.

We did not intend for the 69-channel experiments to access a region of large PCI growth, primarily because of the relatively few number of actuators in the system and the limited dynamic range of the adaptive optics hardware. We did intend, however, for the 69-channel experiments to provide early data for code verification well before the completion of the larger 241-channel system.

The increased number of actuators in the 241-channel system permitted compensation at spatial frequencies approximately twice as high as with the 69-channel system, thereby approximately quadrupling the expected PCI growth rate [10]. In addition to having more channels, the larger system had a greater deflection range, or stroke, on the deformable mirrors, a larger dynamic range of the wavefront sensor, and more flexible phase-reconstruction capabilities to permit the investigation of alternate reconstruction schemes.

A schematic of a generic turbulence/thermal-blooming compensation experiment is shown in Figure 2. In our experiments, we simulated turbulence via transmissive phase screens (produced by ion-etching a fused-silica substrate) of varying turbulence strength ϕ, and we induced thermal blooming with I_2-doped, CCl_4-filled cells of varying absorptivity α. The phase screens were the same diameter as the thermal-blooming cells and could be either used as windows to the blooming cells or separately mounted in rotating frames to provide turbulence simulations at varying altitudes. All blooming cells were approximately 20 cm in diameter, substantially larger than the 1-cm laser beam that propagated through the cells. We simulated wind by rotating the cells and propagated the beam through an outer radius to minimize the variation of the wind across the beam diameter. The experiment was designed to incorporate up to six phase screens and three blooming cells. All of the experiments discussed in this article, however, were conducted without phase screens and with only one blooming cell because our primary purpose was to explore the physics of PCI.

In our experiments, a 0.514-μm beam from a 20-W Ar-ion laser reflected off deformable and tilt-correction mirrors and propagated vertically through the blooming cells. The process created transverse thermal gradients in the blooming medium and the

gradients distorted the outgoing beam. We focused the beam, which was approximately 1 cm in diameter, into a camera at the end of the blooming path to simulate propagation to the far field. This camera provided one of the primary diagnostics for the experiment.

For the adaptive optics beacon, we used a low-power laser beam—a 0.633-μm HeNe laser beam whose diameter was slightly larger than that of the Ar-ion outgoing laser beam. The beacon beam propagated in the opposite direction through the blooming medium and exited the blooming cells with the distortions that the outgoing laser beam had induced. The beacon beam reflected off the tilt-correction and deformable mirrors and was transmitted through a dichroic beam splitter into a wavefront sensor. The sensor measured the phase gradients in a two-dimensional array of subapertures that were registered with the deformable-mirror actuators. The measured gradients thus corresponded to the local x and y tilts between the deformable-mirror actuators.

The wavefront reconstructor converted the phase gradients into phase values centered at each actuator location. The deformable-mirror drivers then used the reconstructor outputs to derive the individual voltages required to produce the desired deflection of the mirror surface at each actuator location. In our experiments, the adaptive optics operated in a continual null-seeking mode in which each actuator was displaced so as to zero the beacon phase at that location. We located the base of the blooming cell, one deformable mirror, and the wavefront sensor at conjugate image planes to minimize the conversion of phase to intensity in the intervening

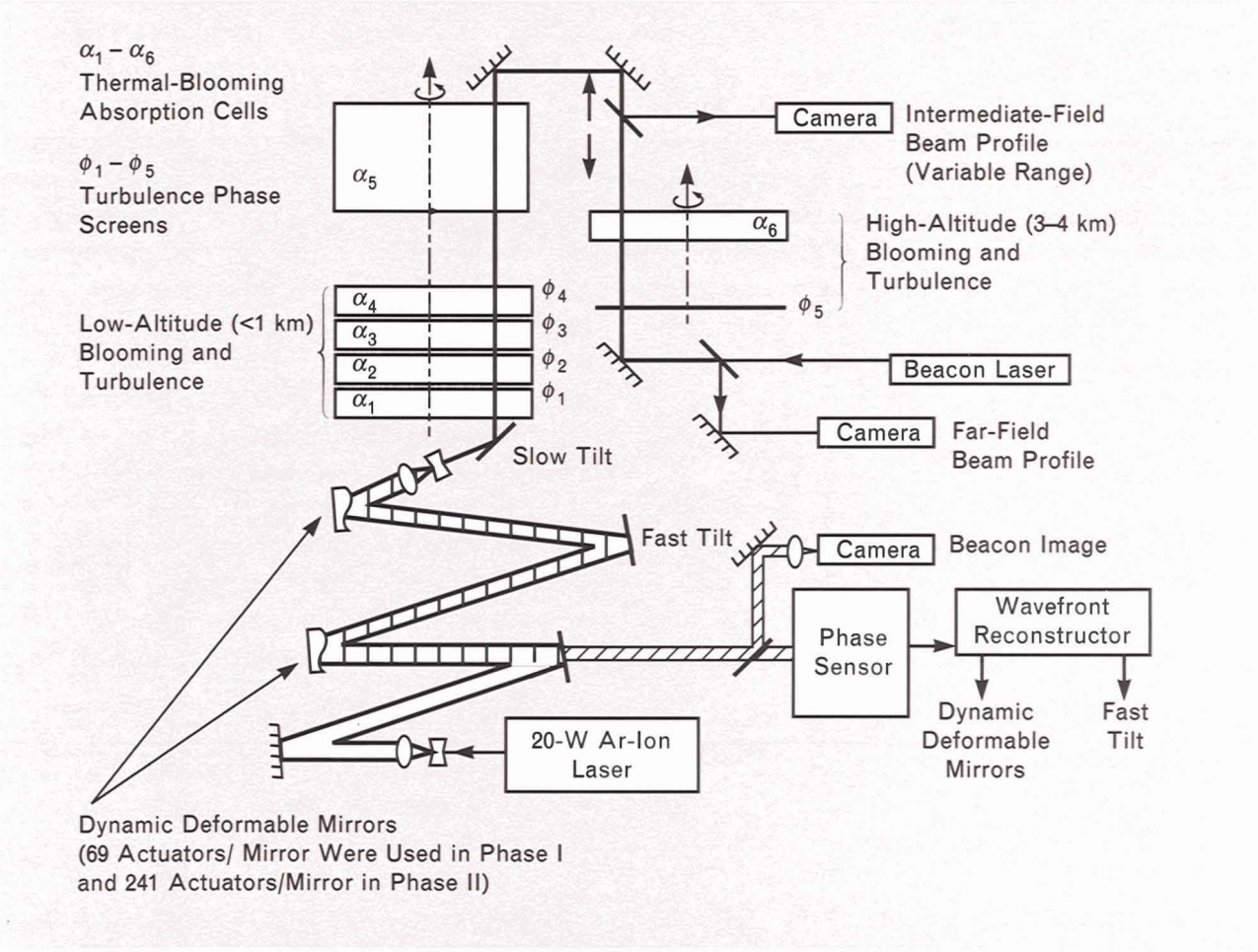

FIGURE 2. Turbulence/thermal-blooming experimental layout.

optical paths. When the adaptive optics system was turned on, the outgoing laser beam entered the blooming cell with the conjugate of the phase the beam would encounter in the blooming medium already applied to the beam.

Tilt compensation was based either on tilt estimates made by the reconstructor or on independent measurements in a tilt-sensing loop that typically contained a quad cell—a position sensor that sensed displacement of the focused beacon. In general, we included two tilt-correcting mirrors in the experimental setup: one mirror responded to the low-frequency (<20 Hz), large-stroke (~10 mrad) tilt that is induced by thermal blooming, while the other mirror responded to the high-frequency (~200 Hz), small-stroke (~100 μrad) tilt that is characteristic of turbulence.

When the compensation was successful, the outgoing laser beam exited the blooming cell with a flat phase and the beam could be brought to a tight focus in the far field. Additional diagnostic cameras were located at the far-field image of the beacon beam, and at various intermediate-field locations along the optical propagation path. We used the intermediate-field cameras mainly to monitor the development of scintillation on the outgoing laser and beacon beams in the presence of PCI. In addition, the measured phase gradients, computed phase, and applied actuator voltages and mirror displacements were all recorded.

Scaling

To determine such experimental characteristics as laser power and beam diameter, we identified scaling parameters that allowed us to simulate, on a laboratory scale with low-power lasers, the degree and type of phase distortion that would be encountered by a large, high-power-laser beam propagating through the atmosphere. Two of these parameters are the distortion number N_D and the perturbation Fresnel number N_P (see the box "The Distortion and Fresnel Numbers"). N_D, which is proportional to the strength of the thermal-blooming phase distortion, determines the required stroke on the deformable mirrors as well as the required dynamic range of the wavefront sensor. N_P describes the effect of diffraction on adaptive-optic-scale sizes and is partially determined by the actuator spacing of the deformable mirror.

An additional consideration in the design of a scaled adaptive optics experiment is the required system bandwidth, which is determined by the smallest time scale during which the (simulated) atmosphere is expected to change. For thermal-blooming compensation, this time scale is defined by a wind-clearing time—the time it takes for wind (either real or slew-induced) to clear the heated atmosphere out of the beam path. In order to reproduce the temporal behavior of larger systems in the real atmosphere, we required in our laboratory experiments that the product of the adaptive optics correction bandwidth and the wind-clearing time be constant. This requirement is almost equivalent to insisting that the wind-clearing time in the laboratory not differ substantially from the wind-clearing times in the atmosphere because most adaptive optics systems to date, both in the laboratory and field, have operated with bandwidths of up to several hundred hertz and we do not anticipate being able to increase that limit substantially in the near future.

Phase I

A photograph of the Phase I experimental layout is shown in Figure 3. In the foreground, a blooming cell is mounted on a tower in which two blooming-cell frames are visible. Note the two 69-channel deformable mirrors in the middle ground. The mirrors are of a monolithic piezoelectric material (MPM) design and they have stroke displacements of about 1.4 μm each. In the background, the wavefront sensor—a radial-grating shearing interferometer that measures $60x$ and $60y$ phase gradients at a 10-kHz frame rate [17]—is visible. The measured gradients were reconstructed in an analog resistor-network reconstructor to yield 69 phase values, which were used in 69 null-seeking loops that operated at bandwidths of 100 Hz. In the Phase I experiments, tilt compensation was performed by a null-seeking tilt loop in which a three-actuator mirror was controlled by tilt estimates derived from the wavefront reconstructor. The racks surrounding the optical bench were all part of the electronics required to operate the mirrors, the wavefront sensor, and the various cameras that comprised the diagnostic equipment.

THE DISTORTION AND FRESNEL NUMBERS

THE DISTORTION NUMBER is defined as [1]

$$N_D = \frac{8\sqrt{2}\pi}{\lambda}\left(\frac{dn}{dT}\frac{1}{\rho c_p}\right)\frac{P_0}{D} \cdot \int_0^L \frac{\alpha(z)}{v(z)+\omega z} H(z)dz,$$

where $H(z) = e^{-\int_0^z [\alpha(z')+\alpha_s(z')]dz'}$.

N_D describes the integrated phase distortion across a beam diameter D that results when a beam of wavelength λ and power P_0 propagates through a medium of length L in the presence of a transverse wind. Note that the term $(dn/dT)[1/(\rho c_p)]$ is determined solely by the density ρ, specific heat c_p, and refractive-index variation with temperature dn/dT of the propagation medium. The term in the integral is the range-dependent absorptance of the medium divided by the wind velocity $v(z)$ or the effective wind velocity $v(z) + \omega z$, α is the attenuation coefficient due to absorption, and α_s is the attenuation coefficient due to scattering.

Obtaining large phase distortions from low-power beams in the laboratory requires a medium for which the quantity $(dn/dT)[1/(\rho c_p)]$ is as large as possible. The medium must also have a low thermal diffusivity so that forced convection (wind) will be the primary cooling mechanism, as it is in air. Gases are not appropriate media for laboratory experiments, as the thermal diffusivity of gases is too high. The diffusive cooling over small, centimeter-size beams is much more severe than the diffusive cooling over the meter-size beams used in atmospheric propagation.

Consequently, we examined several liquids such as water, ethanol, and CCl_4, and compared the dn/dT and diffusivity χ of each. We chose CCl_4 because it had the largest dn/dT and smallest χ of the liquids. Even in CCl_4, however, cooling by thermal diffusion exists to a much larger degree than it does in the atmosphere. In fact, if we were to operate at too slow a wind speed, then cooling by diffusion might dominate cooling by wind. Thus the beam diameter and wind speed were chosen so that heat deposited in size scales of the order of two actuator spacings (discussed in the following paragraph) diffuses by no more than 10% in one wind-clearing time. To satisfy the N_D scaling (see the subsection "Scaling" in the main text), we absorbed approximately 60% of the incident laser power.

The perturbation Fresnel number N_P is defined as

$$N_P = \frac{\pi n d^2}{4\lambda L},$$

where n is the index of refraction, and d is the perturbation scale. We chose d to equal the deformable-mirror Nyquist frequency, which is two actuator spacings. The choice of the perturbation scale came from the prediction that the highest PCI gain will occur at the highest spatial frequency that the adaptive optics can accommodate (nominally two actuator spacings). In general, PCI gain is highest when N_D is large and N_P small.

References

1. L.C. Bradley and J. Herrmann, "Phase Compensation for Thermal Blooming," *Appl. Opt.* **13**, 331 (1974).

Figures 4(a) and 4(b) show contour plots of the far-field irradiance of the Ar-ion outgoing laser beam in both open-loop (i.e., no adaptive optics) and closed-loop (i.e., with adaptive optics) operation. The crescent-shaped profile in open-loop operation (Figure 4[a]) is characteristic of thermal blooming. If there had been no wind, the bloomed beam would have exhibited simple defocus and the far-field irradiance would have appeared symmetrically spread around the center. The presence of a transverse wind intro-

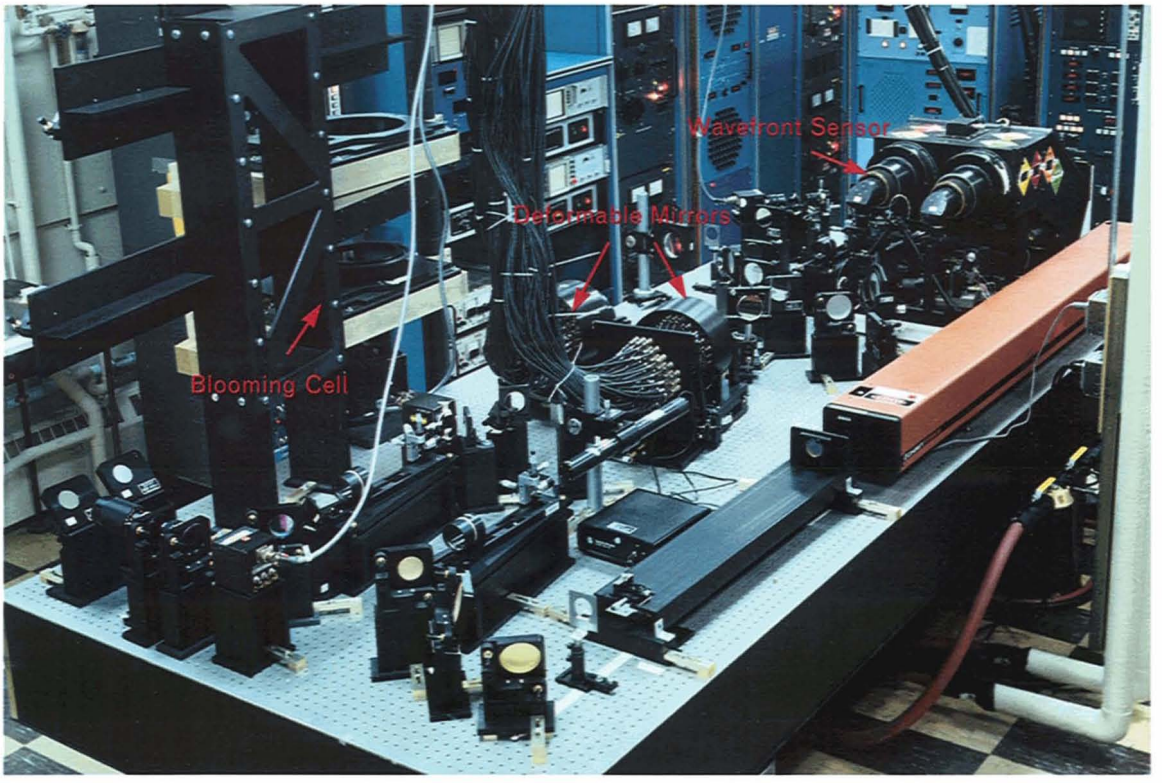

FIGURE 3. Phase I experimental layout.

duces a tilt and also causes the defocus to be stronger in one axis than the other. Thus the resulting phase aberration is largely astigmatic and the far-field irradiance appears as a crescent bent into the wind direction. In contrast, the closed-loop beam (Figure 4[b]) is a well-focused spot whose width is essentially diffraction limited.

We examined the far-field irradiance for a range of N_D, which we varied by changing the laser power. In Figure 5, the open black circles depict the peak irradiances in open-loop operation. Note that the irradiance increases with increasing N_D (laser power) up to a critical point (power) where a further increase in N_D (laser power) results in a decrease in the far-field

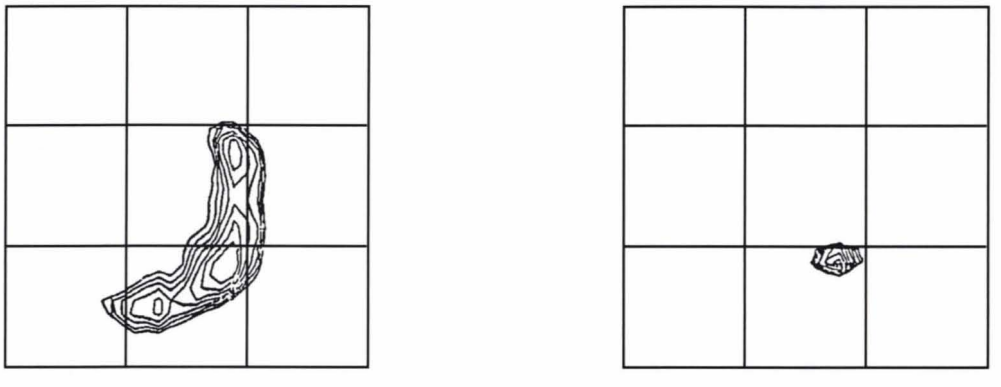

(a) (b)

FIGURE 4. Far-field irradiance of outgoing laser beam in (a) open-loop and (b) closed-loop operation. Note the thermal-blooming-induced crescent shape in part *a*. The beam diameter in part *b* is approximately diffraction limited.

irradiance. The solid black circles represent the peak irradiance in closed-loop operation. Note that with phase compensation, the irradiance has increased by an order of magnitude for higher N_D values, and the critical power has increased by almost an order of magnitude. In closed-loop operation, the critical power occurs at an N_D of nearly 200, at which point the deformable mirrors were at the limit of their stroke capabilities. The red circles and curve are the results of MOLLY simulations of these experiments. Note the excellent agreement, even at the point at which the hardware limits the performance. Thus the Phase I experiments demonstrated stable phase compensation of thermal-blooming distortion and provided data for the first comparison of the time-dependent code with experimental results.

As mentioned previously, we had little expectation of observing the spontaneous onset of PCI in the Phase I experiments. Thus we decided to try to stimulate the instability. We passed the outgoing laser beam through a transmissive mask onto which a sinusoidally varying intensity pattern was imposed at the Nyquist frequency d of the deformable mirror (Figures 6[a] and 6[b]). Our intent was to observe any growth of intensity and/or phase modulations by seeding an intensity perturbation at the frequency that had the highest predicted growth rate. The modulation growth would presumably be caused by PCI.

We examined the near-field irradiance profile of the outgoing laser beam at the top of the blooming cell at the end of one wind-clearing time in both open and closed-loop operation. Figure 7 shows slices of the near-field irradiance profile taken across the center of the beam, perpendicular to the wind direction, for an incident laser power of 0.9 W (N_D = 85 and N_P = 120). In open-loop operation, the initial modulations were smeared out due to thermal blooming. But in closed-loop operation, the modulations were enhanced, and the enhancement increased with increasing laser power (see the box "Low- and High-Spatial-Frequency Modulation"). To quantify the growth or decay of the modulations more easily, we Fourier-transformed the slices and plotted the component of the power spectrum at the modulation frequency as a function of time (Figure 8). As expected, the modulation depth was the same for both open- and closed-loop operation at time zero. But, although the modulations decayed quickly in open-loop operation, they grew in closed-loop operation. Growth of the modulation reached a steady-state saturation value in a time that depended on the slice examined (Figure 6[a]). For a slice in the center of the beam, saturation occurred at one-half the wind-clearing time. For slices upwind of center, saturation occurred earlier; for slices downwind, saturation occurred later.

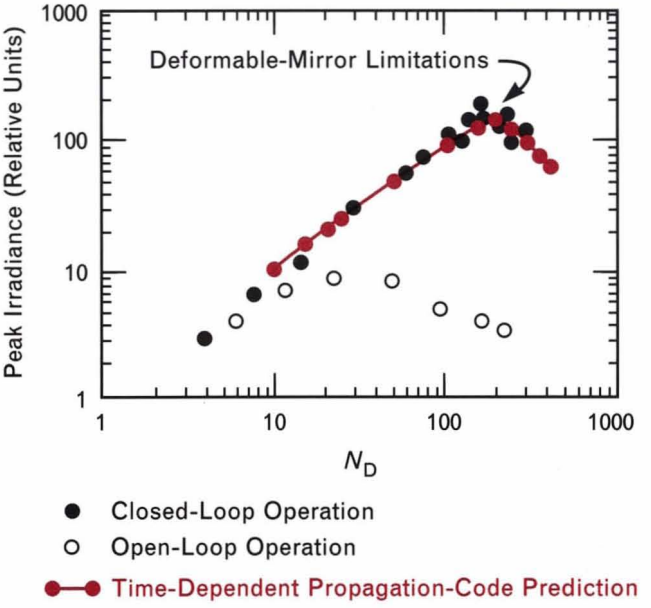

FIGURE 5. Peak irradiance as a function of N_D in both open- and closed-loop operation. The red data points and curve are the results of simulations by MOLLY, a time-dependent propagation code. Note the excellent agreement with the closed-loop results.

We also examined the phase that was applied to the deformable mirror at the end of one wind-clearing time. A clear signature of PCI is growth of a structure at a Nyquist frequency on the deformable mirror. It is this growth, of course, that drives the intensity modulations described above. If the PCI growth is fairly small, then we can often use a linearized theory to predict the gain, i.e., the modulation growth in one wind-clearing time, due to the instability.

The circles in Figure 9 show the amplitude of a ripple at the Nyquist frequency (observed in the phase applied to the deformable mirror) as a function of position on the mirror from upwind to downwind.

(Linearized theory predicts identical growth rates of PCI for both the intensity modulation observed in the beam frame and the applied-phase modulations observed in the mirror frame.) In Figure 9, the blue dashed curve is the calculated phase growth that would occur in the absence of PCI; this growth results simply from compensation for the accumulated heating, integrated from upwind to downwind, of the modulated-input intensity. Note that the actual phase growth is noticeably higher than the zero-gain limit and the growth is in good agreement with that predicted by linearized-gain theory (the blue solid curve). As before, the red curve denotes the MOLLY predictions, which are in excellent agreement with both the linearized-gain theory and the measurements.

In these experiments, we obtained what we believe to be the first experimental evidence of PCI. This instability was difficult to excite; it required both seeding with a large modulation and careful alignment of the modulation with the actuator grid and wind direction. Results of these experiments were in good agreement with time-dependent code predictions and provided ample motivation for the Phase II investigations of spontaneous PCI in a high-gain region.

Phase II

Experimental Hardware

With the exception of the blooming cells and some relay optics, almost all hardware for the Phase II experiments (Figure 10) was newly procured. As stated earlier, one goal of the Phase II system was to access a region of high PCI gain. Thus the deformable mirrors had more stroke and actuators, and the wavefront sensor had a greater dynamic range.

The 241-channel, low-voltage electrostrictive material (LVEM) deformable mirrors (Figure 11) [18] were built by Itek. The deformable mirrors had a combined maximum stroke of about 7 μm and a combined maximum interactuator-stroke difference of approximately 3 μm. The interactuator-stroke limits resulted from protective circuitry implemented to avoid overly stressing the mirror facesheet.

Deformable mirrors typically have an inherent structure in the form of a dimpling, which can be produced during the facesheet-polishing process, at the actuator locations. This structure can usually be kept smaller than $\lambda/20$ rms, in which case its presence does

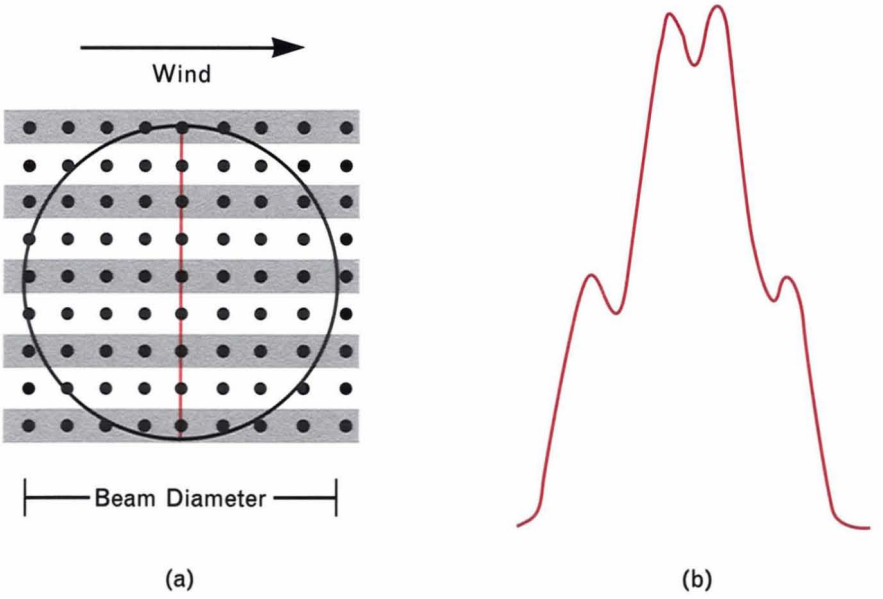

FIGURE 6. Imposed intensity perturbation to seed PCI: (a) geometry of intensity-modulation mask in which dots correspond to positions of deformable-mirror actuators and the center line indicates the position of irradiance scan of part *b*, and (b) measured laser irradiance profile perpendicular to modulation direction.

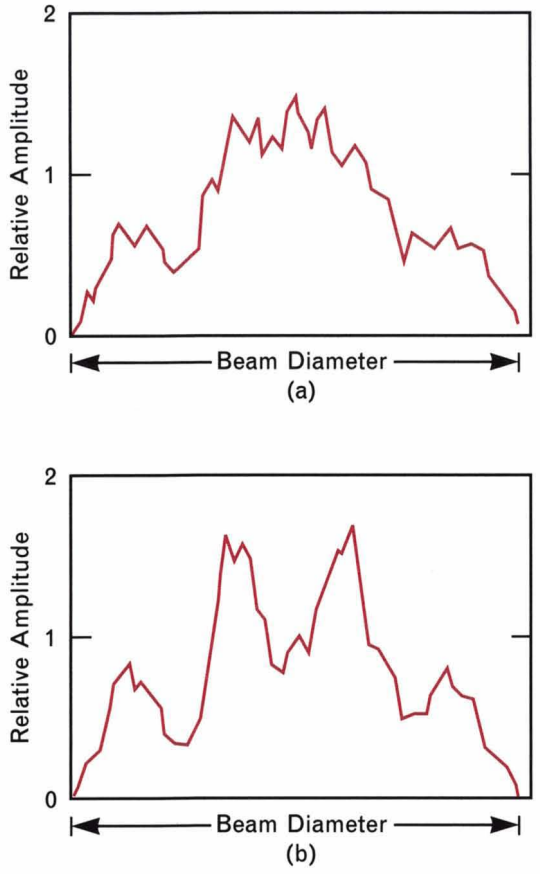

FIGURE 7. Irradiance of outgoing laser beam at the end of one wind-clearing time in (a) open- and (b) closed-loop operation.

not significantly affect the beam propagation. In addition to this dimpling, the Phase II deformable mirrors had a surface structure that occurred approximately at the Nyquist frequency but was 90° out of phase with the actuator locations (i.e., the peaks and valleys of the structure fell between the actuator locations). The surface structure was as high as $\lambda/10$ peak-to-peak in some places, and it represented an uncorrectable source of residual-phase error due to its positioning. We believe that the residual structure, which increased with increasing overall stroke on the mirror, originated from nonuniformities within the actuators themselves. Thus, instead of producing straight piston responses to applied voltages, the actuators could sometimes bend, creating dimples or bumps between actuators. Understanding this structure became essential to interpreting the experimental results, discussed later in this section. (Note: The structure provided valuable information on the manufacturing requirements for deformable mirrors. In fact, this problem was identified early enough and the actuator-fabrication process changed so that the deformable mirror built for the SABLE experiments [12] does not exhibit this feature.)

The wavefront sensor (Figure 12), also built by Itek, was a radial-grating shearing interferometer [16] that was similar in design to the interferometer of Phase I and that measured $224x$ and $224y$ phase gradients at a 10-kHz frame rate. The maximum dynamic range of the wavefront sensor was $\pm 6.5\lambda$ per subaperture, which was a threefold increase over the dynamic range of the Phase I sensor. A 16-bit digital reconstructor [19], built at Lincoln Laboratory, converted the measured phase gradients into phase values centered at each actuator. The reconstructed phases were converted to mirror-drive signals in the servo compensators, which were also built at Lincoln Laboratory. The servo compensators had a number of new features that allowed, for example, the addition or removal of a stored surface figure to correct for static systematic wavefront aberrations.

In contrast to the procedure used in the Phase I experiments, tilt compensation was performed by an independent tilt loop and not by signals derived from the reconstructor-tilt estimates. In the new setup, a portion of the beacon beam was split off after exiting the blooming cell and focused into a position sensor. The x and y position signals were sent to a four-actuator, 16-mm-aperture mirror that was driven to

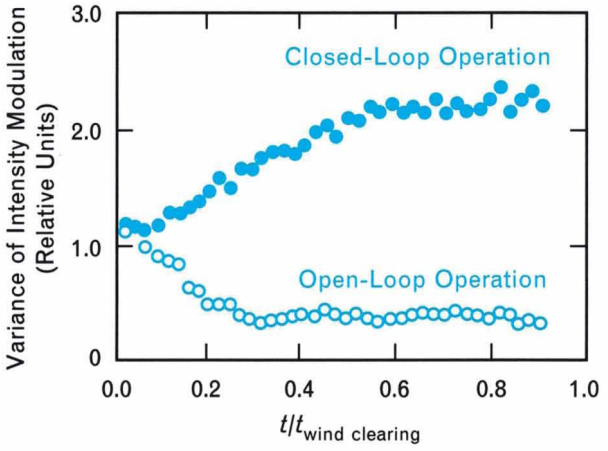

FIGURE 8. Intensity modulation at Nyquist frequency as a function of time (N_D = 85 and N_P = 120).

LOW- AND HIGH-SPATIAL-FREQUENCY MODULATION

THE SPATIAL FREQUENCY of the modulations that we imposed to seed phase-compensation instability (PCI) was fairly low, limited to what the deformable mirror could correct. We also conducted several experiments to observe the open-loop behavior of modulations at high spatial frequencies (i.e., beyond the compensation range of the deformable mirrors). Intensity modulations in these two regions are expected to evolve along the propagation path in distinctly different ways.

At low spatial frequencies (i.e., large Fresnel numbers), the evolution is dictated almost entirely by the strength of the thermal blooming. As shown in Figure 7(a) in the main text, blooming will cause these modulations to smear out.

At high spatial frequencies (i.e., small Fresnel numbers), the evolution of modulations is affected not only by blooming but by dif-

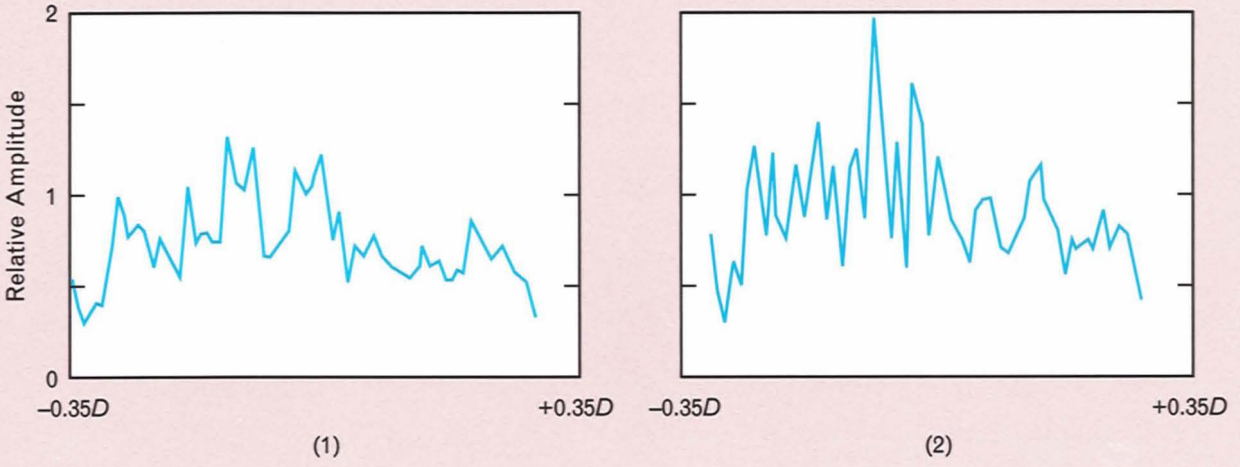

FIGURE A. Outgoing-beam irradiance in open-loop operation at (a) time zero and (b) about one-tenth the wind-clearing time later. (Note: *D* is the beam diameter.)

maintain zero displacement at the position sensor.

The Phase II Experiments

Except as mentioned, we conducted most of the experiments by closing the loops around the beacon beam for several wind-clearing times before opening a shutter to transmit the Ar-ion outgoing laser beam. A ground-based laser system would presumably use this mode of operation because of the difficulty of maintaining a high-energy laser in a constant On mode. (Note: This mode is sometimes referred to as the *ab initio* mode because the adaptive optics loops are closed from the start. An alternate mode, in which the beam is first shuttered on, blooming is allowed to develop fully, and then the loops are closed, is called the *deferred* mode.) Our experiments were aimed at observing PCI signatures, which are described in the article by Jonathan F. Schonfeld [20] in this issue. Briefly stated, these signatures are rippling of the deformable mirror at a Nyquist frequency, characteristic pattern formations on the outgoing laser and beacon beams, and a significant decrease in the (compensated) far-field irradiance with increasing N_D. It is worth mentioning that these signatures were initially derived with ideal adaptive optics models. We expected that the behavior of real hardware would influ-

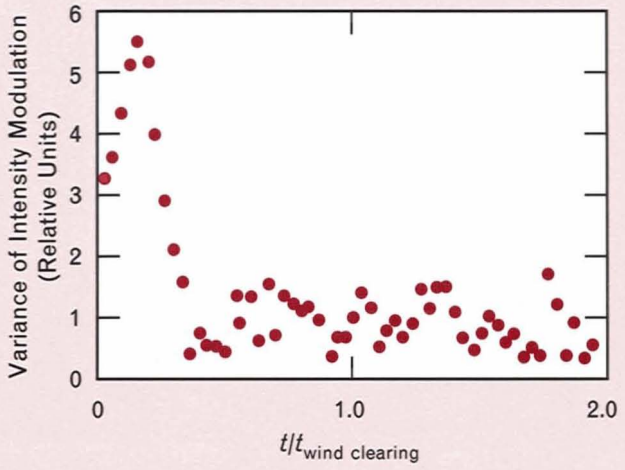

FIGURE B. Intensity modulation at a high spatial frequency as a function of time (N_D = 66 and N_P = 0.8).

fraction as well. Light from individual intensity ripples will spread at relatively large angles, and, if the blooming layer is thick enough, rays from different ripples will intersect and lead to multiple regions of interference and enhanced modulation. If we examine a transverse slice of the beam irradiance at a fixed propagation distance far from the transmitter, the modulations will appear to grow in time until their growth is saturated by some mechanism.

To observe this growth, we modulated the intensity of the outgoing laser beam with a mask whose dominant frequency component was approximately four times higher than that used for the PCI-seeded experiments. Figure A(1) shows a slice of the irradiance profile at time zero when the beam is turned on, and Figure A(2) shows the slice at about one-tenth of a wind-clearing time later as blooming develops. Note the growth of the high-spatial-frequency structure at the later time. Figure B displays the Fourier component of the power spectrum of this irradiance slice as a function of time. As predicted, the modulation depth grows until it reaches a peak, where further growth is probably limited by thermal diffusion. The modulation is then smeared by thermal blooming until wind clears the beam.

This rapid and large initial growth of high-spatial-frequency modulation is similar to what might be expected for a high-distortion-number beam propagating through turbulence. Turbulence-induced scintillations can provide initial high-spatial-frequency modulations, which are referred to as hot spots (see the section "Motivation" in the main text). As the modulations grow, they scatter energy out of the beam and can sometimes result in a significant decay of the far-field irradiance.

ence these signatures; as will be shown, we were not disappointed.

Observations of rippling on the deformable mirror. Figure 13 shows the measured deformable-mirror strokes at the end of one wind-clearing time for an incident laser power of 3.8 W (N_D = 280 and $N_P \approx 10$). Note that the Nyquist-frequency rippling is greatest in the downwind-center portion of the mirror, where PCI has had the longest time to develop and where the beam intensity is greatest. At an incident laser power of 3.8 W, the maximum peak-to-peak deformation of the mirror surface grew to about 5λ. It is interesting to note that a steady-state condition was not achieved; i.e., the rippling on the deformable mirror continued to change as the adaptive optics system responded to an ever-changing heating profile in the blooming medium. This observation of rippling on the deformable mirror was, to our knowledge, the first experimental evidence for spontaneous growth of PCI.

Because PCI increases with spatial frequency, the ripples occur preferentially at the highest spatial frequency that the actuator grid can support. In the absence of wind, this frequency occurs at 45° to the grid at a period of $\sqrt{2}a$ where a is the actuator spacing (Figure 14). For winds aligned along the grid axis,

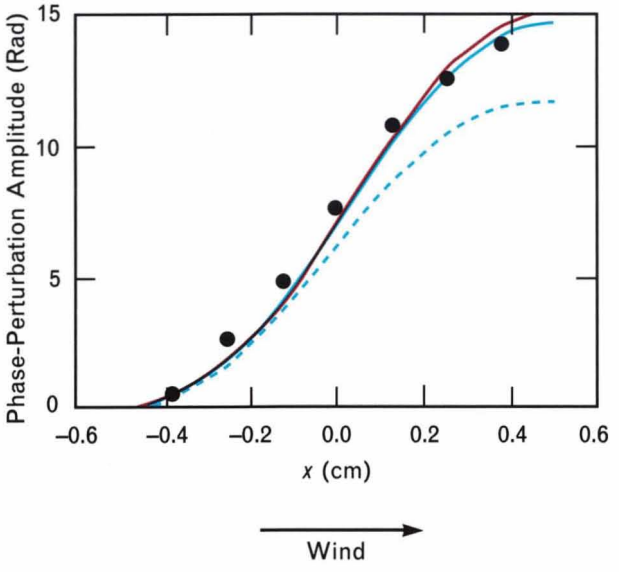

FIGURE 9. Magnitude of phase ripple in center of beam at the end of one wind-clearing time. The black circles represent measured data points; the blue dashed curve is the calculated growth in the zero-gain limit, i.e., the growth that would occur in the absence of PCI; the blue solid curve is the calculated growth from linearized-gain theory; and the red curve represents results from MOLLY simulations.

as in our experiments, the angle of dominant ripple formation is reduced somewhat and the period is slightly larger.

To quantify the growth of the deformable-mirror ripple and to examine it as a function of laser power, we define a quantity that is related to the Nyquist-frequency rippling at 45° to the actuator grid. If we envision the deformable-mirror surface as a checkerboard with the light and dark squares centered on alternating actuators, we can assign each actuator to a diagonal row on the actuator grid. For each frame of deformable-mirror data, we can take the sum of all the strokes on the light squares and subtract it from the sum of all the strokes on the dark squares, and this difference will be a measure of the total stroke modulation at 45° to the grid. The black circles and squares in Figure 15 display the maximum value of this difference in the first wind-clearing time for two experimental runs over a range of laser powers from zero to about 4.6 W (N_D = 340). Note the almost sixfold increase in this ripple growth as the laser power is increased from 2 to 4 W. This growth is a clear sign of PCI.

At approximately 4 W, the deformable mirrors were driven to the limit of their stroke capability, and the scintillations on the beacon beam exceeded the intensity dynamic range of the wavefront sensor. Although one might have expected the ripple amplitude to saturate at these hardware limits, Figure 15 shows that the amplitude (i.e., the PCI signature) actually dropped at powers greater than 4 W. The drop occurred because the wavefront sensor failed to deliver meaningful data for intensities significantly beyond the dynamic range for which it was designed, and the adaptive optics system effectively performed no phase compensation at all. Hence there was a resulting reduction in instability growth (as well as in any blooming compensation).

Early simulations of this experiment with the time-dependent propagation code MOLLY predicted much larger growth than was actually observed, and we began to suspect that the residual-phase structure on the deformable mirror was influencing our experimental results. MOLLY already included realistic models for the influence of individual actuators on neighboring actuators, but the residual structure was contributing a different type of error whose effect was to suppress the feedback between the blooming medium and the adaptive optics system. In other words, the difference between the actual applied phase and the intended applied phase was large enough so that the growth of PCI was suppressed.

To test this hypothesis, we recorded interferograms of the deformable-mirror surfaces after applying a precalculated thermal-blooming surface figure for a moderately high blooming level ($N_D \approx 240$). We then calculated the residual phase (measured phase minus intended blooming surface figure) and formed a 288×288 array of phase values to be used as inputs to the computer model. The residual-phase array formed a phase screen that was located, in the computer model, at an image plane of the deformable mirror. Each propagation iteration would first apply the stored phase aberration to the beam and then propagate the beam through the cell to mimic the effect of the phase structure on a real beam reflecting off the deformable mirror. The red data points and curve in Figure 15 represent a MOLLY run with this residual-phase structure included. Note the excellent

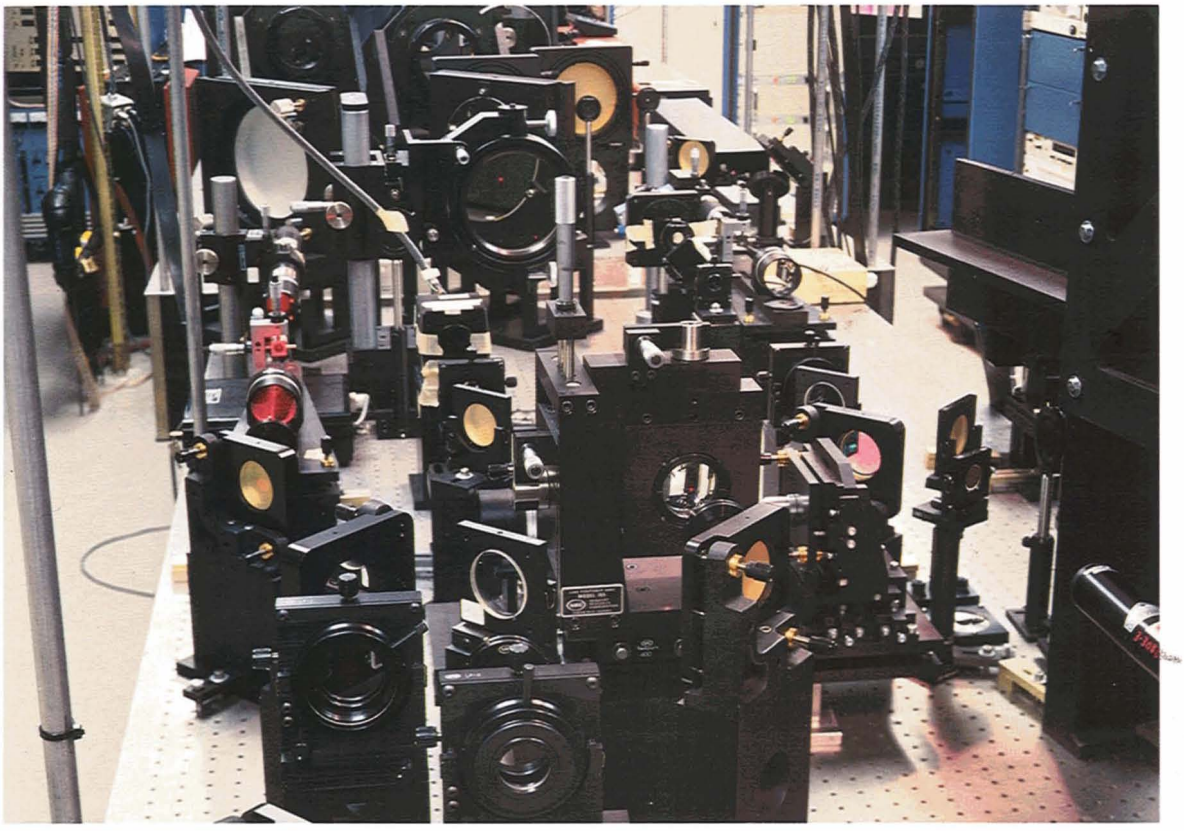

FIGURE 10. Phase II experimental layout.

agreement with the experimental results up to the laser power at which the hardware limits were reached. Thus we obtained the first experimental evidence of how the specific characteristics of the adaptive optics hardware influence high-energy-laser beam propagation, and we could successfully incorporate the relevant features into the code.

Characteristic pattern formations. A second PCI signature—pattern formation on the outgoing laser and beacon beams—can be seen in Figure 16(a). The figure displays the beacon irradiance measured at the base of the blooming cell (i.e., the bottom of the "atmosphere") at the end of one wind-clearing time for an $N_D \approx 300$. Note the diamond-shaped structure in the upper right quadrant of the photo. The orientation and aspect ratio of the structure match that predicted by theory and by MOLLY runs with ideal adaptive optics (Figure 13 in the article by Schonfeld [20] in this issue). The pattern is corrupted elsewhere because of deformable-mirror defects such as failed actuators (both mirrors had several) and residual phase structure. When these defects were included in MOLLY, the resulting irradiance (Figure 16[b]) showed remarkable similarity to the measured distribution. The observation of pattern formation in the presence of PCI was an experimental first. Furthermore, the credibility of the code was enhanced con-

FIGURE 11. 241-channel deformable mirrors of Phase II experimental layout.

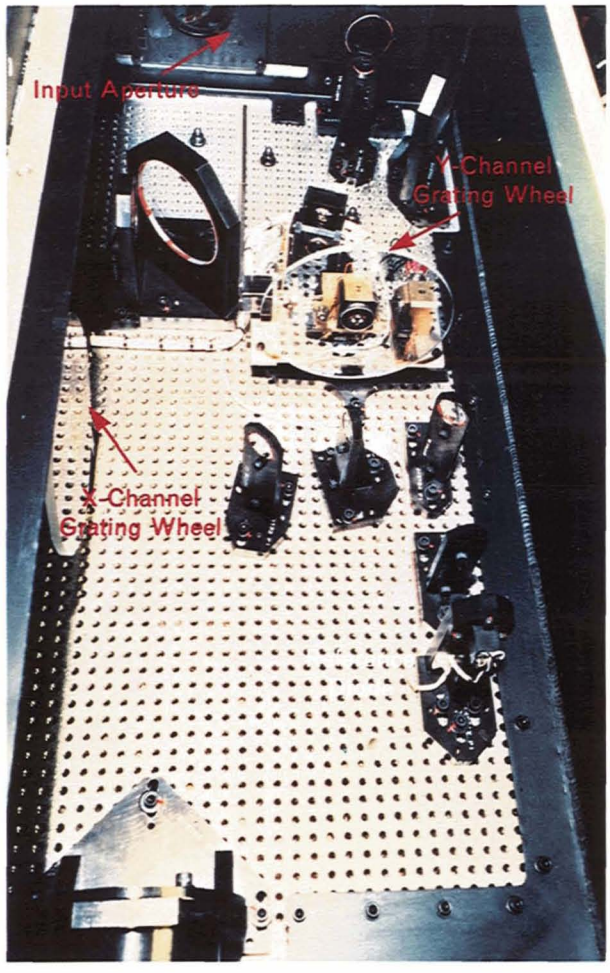

FIGURE 12. Wavefront-sensor optical unit of Phase II experimental layout.

siderably by its ability to reproduce the qualitative and quantitative features of the experimental observations with such accuracy.

Far-field irradiance decay. We found the third signature of PCI by examining the far-field irradiance as a function of laser power. Figure 17 displays the ratios of the peak irradiance at two wind-clearing times after the outgoing laser beam is turned on to the peak irradiance when the beam is first shuttered on. The black circles, diamonds, and squares are from three experimental runs, and the red circles and solid curve are from a computer simulation that included the residual-phase error mentioned earlier. Note that the ratio of the irradiances decreases with increasing laser power and plateaus at about 4 W, the power level at which the adaptive optics hardware limits were reached. Also note that the irradiance exhibits a gradual decay

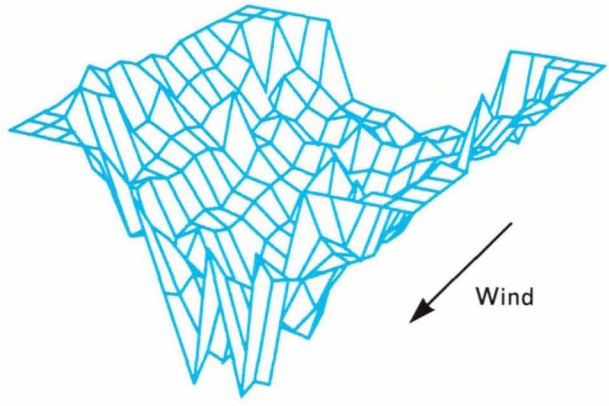

FIGURE 13. Applied-deformable-mirror phase at the end of one wind-clearing time for a laser power of 3.8 W.

that starts at relatively low power levels, as opposed to the sharp roll-off that was observed in computer simulations with ideal adaptive optics (the red dashed curve in Figure 17). The decay begins at low power levels, which suggests that, in addition to PCI, blooming from the residual deformable-mirror structure also contributes to the decrease in far-field irradiance.

To identify how much of the irradiance decrease was caused by PCI and how much was caused by imperfections in the deformable mirrors, we repeated

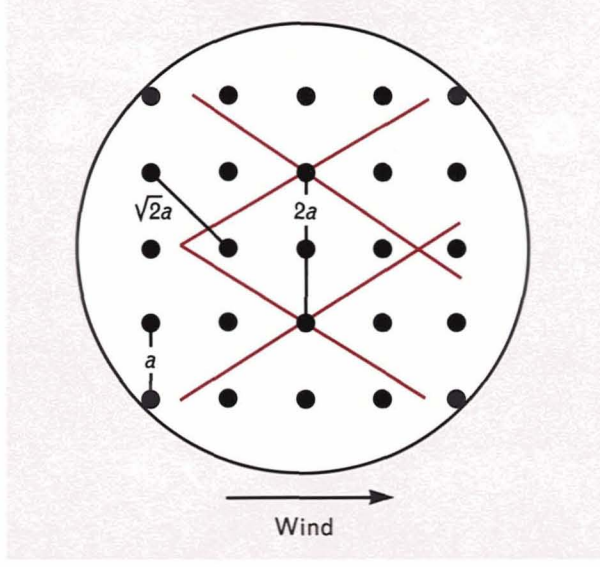

FIGURE 14. Section of actuator grid where actuator spacing along grid axes is denoted by *a*. The red lines illustrate the predicted pattern formation for wind aligned along the grid.

the above experiments in the mode in which blooming was allowed to develop fully *before* the adaptive optics loops were closed. We reasoned that, even in open-loop operation, small-scale blooming from the deformable mirrors would cause a reduction in the far-field irradiance. After the loops were closed, any *additional* decay in the irradiance with elapsed time would be due principally to the adaptive optics feedback, i.e., to the effects of PCI.

Thus we compared the far-field irradiances at the instant of loop closure with the irradiances observed at later times. The two sets of data shown in Figure 18 correspond to the Strehl ratio at loop closure and at the end of two wind-clearing times. (Note: The Strehl ratio is the ratio of the peak irradiance in a given far-field energy distribution to the peak irradiance that would exist if the distribution were produced by a diffraction-limited system.) The Strehl ratios measured at the instant the loops were closed decrease with increasing laser power as a result of small-scale

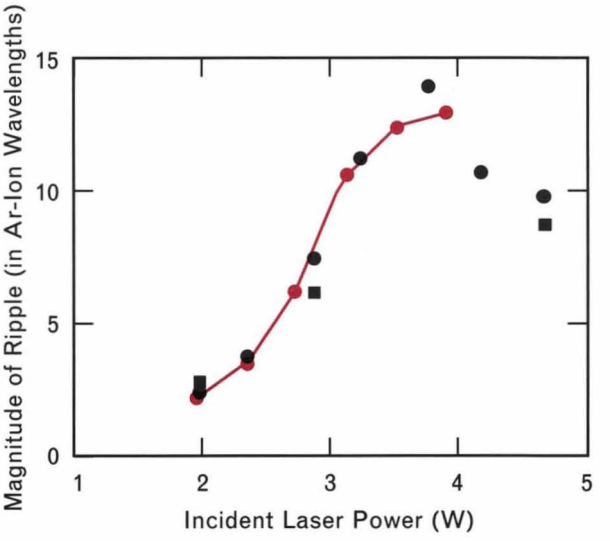

FIGURE 15. Growth of applied Nyquist-frequency phase ripple at 45° to the actuator grid. The black circles and squares represent measured data points from two different experimental runs, and the red circles and curve are from MOLLY simulations that included the residual deformable-mirror structure.

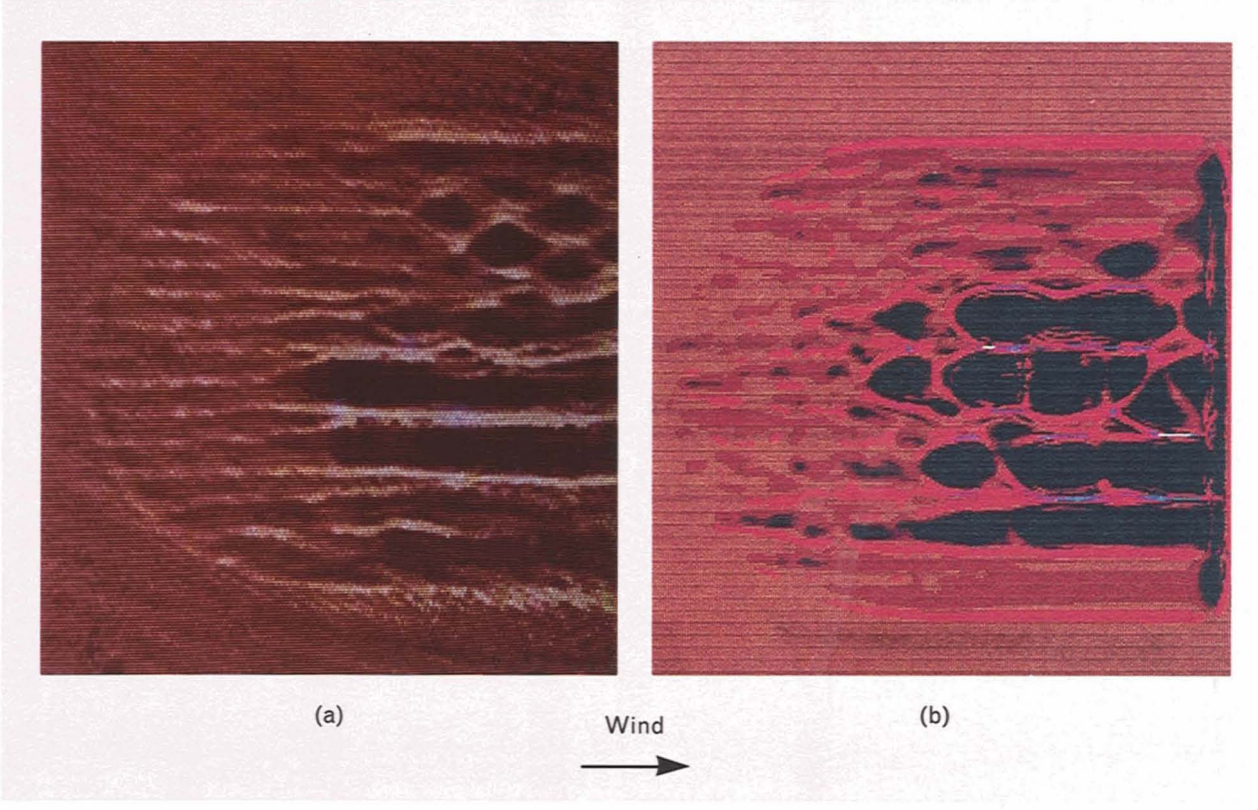

FIGURE 16. Irradiance profile of beacon beam at the base of the blooming cell at the end of one wind-clearing time: (a) measured profile (note the formation of a honeycomb pattern in the upper right quadrant of the image), and (b) MOLLY simulation of profile. A residual-surface structure on the deformable mirrors was included in the simulations.

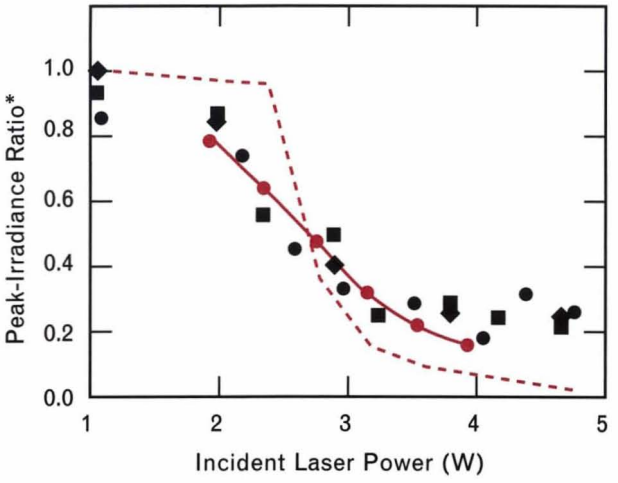

*Ratio of the peak irradiance at two wind-clearing times after the beam is first shuttered on to the peak irradiance when the beam is first shuttered on.

FIGURE 17. Peak-irradiance ratio as a function of laser power. The black circles, squares, and diamonds represent measured values from three experimental runs; the red circles and solid curve are from MOLLY simulations; and the dashed red curve is from MOLLY simulations before a residual-deformable-mirror structure was included.

blooming that arose from the residual deformable-mirror structure. The dependence on laser power, however, was much more pronounced for Strehl ratios measured at the end of the second wind-clearing time, particularly for laser powers above about 2 W. This behavior is characteristic of PCI.

Thus the Phase II experiments provided the first conclusive evidence of the existence of spontaneous PCI. We have seen each of the three PCI signatures in our laboratory and have compared the results of our observations with code predictions. The agreement was excellent when the details of the adaptive optics hardware were taken into account in the modeling.

It is important to note that we optimized these experiments to observe PCI. Even small departures from that optimization, such as tiny misalignments between the beacon and outgoing laser beams, were enough to suppress PCI significantly. Many features of real atmospheric propagation that we did not simulate in the laboratory—e.g., turbulent diffusion, wind variations, slewing of the beam, and variable absorption—are also expected to suppress PCI.

Thus we do not expect that ground-based lasers operating in the real atmosphere will exhibit the strong PCI signatures that were observed in the laboratory. In fact, MOLLY predictions, which do include realistic atmospheric features, indicate that adaptive optics can be effectively used for high-power lasers over a ground-to-space path.

Summary

We have carried out scaled laboratory experiments to investigate phenomena associated with phase compensation of laser beams in the presence of strong thermal blooming. The propagation of a high-energy laser beam through the atmosphere was simulated by transmitting the beam from a low-power laboratory laser through a cell containing an absorbing liquid. Rotation of the cell produced an effective crosswind.

The experiments reported here were directed at observing and quantifying the behavior of a phase-compensation instability (PCI) that had been predicted by propagation codes and analyses. PCI, which results from the positive feedback between the adaptive optics system and the intensity-induced refractivity of the atmosphere, can limit the amount of power that can be usefully propagated through the atmosphere to space. In the experiments, we observed three types of signatures that characterize PCI. The agreement between laboratory results and the predic-

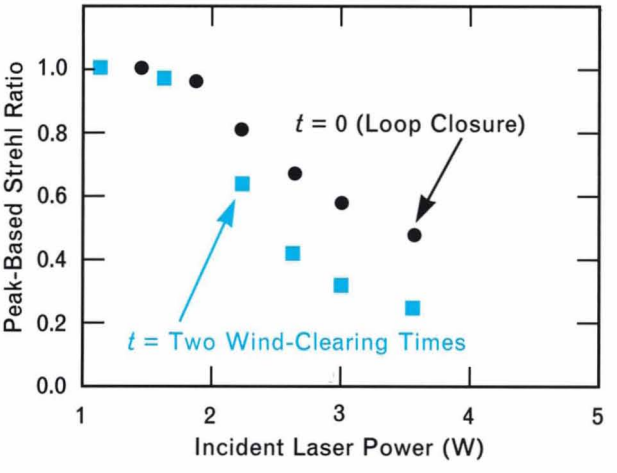

FIGURE 18. Strehl ratio as a function of laser power when loops are first closed (circles) and two wind-clearing times later (squares). (Note: The Strehl ratio is the ratio of the peak irradiance in a given far-field energy distribution to the peak irradiance that would exist if the distribution were produced by a diffraction-limited system.)

tions of MOLLY (Lincoln Laboratory's time-dependent propagation code) was excellent in all cases. The experiments helped benchmark the code, and they provided valuable insight on the importance of including realistic hardware models in the computer simulations.

Acknowledgments

Many people were involved in the design and performance of these experiments. Special gratitude goes to John Vivilecchia for his assistance in the laboratory; Alan Plaut and Jim Eggert for their work on the new deformable mirrors and wavefront sensor; Prescott Grey, Matt Singer, Bob Morse, Bob Freehart, and Sam Rosenberg for the data-acquisition systems and their corresponding electronics; Jim Mooney for the reconstructor; Kevin Witt for the deformable-mirror drivers and for his help in the laboratory; Brian Player for his electronics assistance; and Greg Loney for the tilt-compensation mirror and electronics. Additional thanks are extended to Jonathan Schonfeld, Stephen Grasberger, and Mike O'Brien for the computer-modeling support for these experiments, and to Marty Brennan and Harry Sagarian for their data processing assistance.

This research was sponsored by the SDIO and Army SDC through the Air Force.

REFERENCES

1. D.P. Greenwood and C.A. Primmerman, "Adaptive Optics Research at Lincoln Laboratory," in this issue.
2. D.V. Murphy, "Atmospheric-Turbulence Compensation Experiments Using Cooperative Beacons," in this issue.
3. R.A. Humphreys, L.C. Bradley, and J. Herrmann, "Sodium-Layer Synthetic Beacons for Adaptive Optics," in this issue.
4. B.G. Zollars, "Atmospheric-Turbulence Compensation Experiments Using Synthetic Beacons," in this issue.
5. L.C. Bradley and J. Herrmann, "Phase Compensation for Thermal Blooming," *Appl. Opt.* **13**, 331 (1974).
6. C.A. Primmerman and D.G. Fouche, "Thermal-Blooming Compensation: Experimental Observations Using a Deformable-Mirror System," *Appl. Opt.* **15**, 990 (1976).
7. C.A. Primmerman, F.B. Johnson, and I. Wigdor, "Thermal-Blooming Compensation Using the CLASP System," *Appl. Opt.* **17**, 2909 (1978).
8. J. Herrmann, "Properties of Phase Conjugate Adaptive Optical Systems," *J. Opt. Soc. Am.* **67**, 290 (1977).
9. R. Briggs, "Models of High Spatial Frequency Thermal Blooming Instabilities," Lawrence Livermore National Laboratory Rep. UCID-21118 (LLNL, Livermore, CA, 1987).
10. T.J. Karr, "Thermal Blooming Compensation Instabilities," *J. Opt. Soc. Am. A* **6**, 1038 (1989).
11. J. Schonfeld, "Analysis and Modeling of Thermal-Blooming Compensation," *Proc. SPIE* **1221**, 118 (1990).
12. Private communication.
13. B. Johnson and C.A. Primmerman, "Experimental Observation of Thermal-Blooming Phase-Compensation Instability," *Opt. Lett.* **14**, 639 (1989).
14. B. Johnson and J.F. Schonfeld, "Demonstration of Spontaneous Thermal-Blooming Phase-Compensation Instability," *Opt. Lett.* **16**, 1258 (1991).
15. N.M. Kroll and P.L. Kelley, "Temporal and Spatial Gain in Stimulated Light Scattering," *Phys. Rev.* **A4**, 763 (1971).
16. C.L. Koliopoulos, "Radial Grating Lateral Shear Heterodyne Interferometer," *Appl. Opt.* **19**, 1523 (1980).
17. J. Feinlieb, S.G. Lipson, and P.F. Cone, "Monolithic Piezoelectric Mirror for Wavefront Corrections" *Appl. Phys. Lett.* **25**, 311 (1974).
18. M.A. Ealey and J.F. Washeba, "Continuous Facesheet Low-Voltage Deformable Mirrors," *Opt. Eng.* **29**, 1191 (1990).
19. R.J. Sasiela and J.G. Mooney, "An Optical Phase Reconstructor Based on Using a Multiplier-Accumulator Approach," *Proc. SPIE* **551**, 170 (1985).
20. J.F. Schonfeld, "The Theory of Compensated Laser Propagation through Strong Thermal Blooming," in this issue.

BERNADETTE JOHNSON is a staff member in the High-Energy-Laser Beam Control and Propagation Group, where her focus of research has been in adaptive optics. Before joining Lincoln Laboratory six years ago, she worked for Applied Science Technology and the Argonne National Labs. She received the following degrees: a B.S. in physics from Dickinson College and the University of Heidelberg in Germany, an M.S. in condensed matter theory from Georgetown University, and a Ph.D. in plasma physics from Dartmouth College.